Thin shell foundations: Quantification of embodied carbon reduction through materially efficient geometry

Architecture, Structures and Construction
https://doi.org/10.1007/s44150-023-00101-z

ORIGINAL PAPER

Thin shell foundations: Quantification of embodied carbon reduction through materially efficient geometry

Kiley Feickert[1] · **Caitlin T. Mueller**[1]

Received: 9 December 2022 / Accepted: 4 October 2023

Abstract

Building foundation systems are a significant but understudied contributor to embodied carbon emissions of the built environment, and typically use excess material in prismatic, bending-dominated typologies. This paper identifies and characterizes a promising pathway for reducing the embodied carbon associated with reinforced concrete shallow foundations through an alternative typology, thin shell foundations. The main focus is a quantification and comparison of the environmental impact of typical spread footings and materially efficient shell foundations. Validated analytical engineering equations are applied in a parametric design workflow for the same design load and soil bearing capacity. By iterating through this workflow systematically, insights are gained regarding the applicability of shell foundations to various building typologies and site conditions. Results show that for small column loads and weak soils, shells reduce embodied carbon by about half compared to spread footings. For high applied loads, shells significantly outperform their prismatic counterparts, reducing the environmental impact by almost two-thirds. Foundations are then considered within the context of a whole building structural frame to determine the potential downstream savings when multiple systems are optimized to reduce material use and mass. When floor slabs are shape-optimized in addition to using shell foundations, a building structural system can be constructed for nearly one-quarter of the embodied carbon of a typical system. To take advantage of these potential savings, a method for fabricating thin shell foundations, where earth is compacted and milled to create the formwork, is presented following a review of digital fabrication methods.

Keywords Thin shell foundations · Low embodied carbon · Concrete shells · Digital fabrication · Robotic manufacturing

Introduction

Due to increasing global population, floor area is expected to double by 2070 [1]. At the same time, the building sector contributes 40% of global energy-related carbon dioxide (CO_2e) emissions annually, with embodied carbon contributing 13% as a result of current construction practices [2]. The impact of a buildings structure is significant, accounting for over 50% of the embodied carbon on a project [3]. Therefore, reducing carbon emissions from building structures will play a critical role in limiting global warming to 1.5 °C above pre-industrial levels and creating a more equitable future. This research aims to reduce carbon emissions associated with reinforced concrete foundations by utilizing efficient geometry while addressing the need for a significant increase in adequate housing due to rapid urbanization.

Foundations are a highly impactful contributor to the embodied carbon emissions of a building's structural system, accounting for up to 42% on average [4]. Historically, materially efficient shell foundations have been built and studied for their ability to save cost. In this research, existing analytical equations are applied in a parametric design workflow to evaluate the environmental impact of conventional prismatic foundations (spread footings) and shell foundations for the same design loads to demonstrate that a significant saving to a building's overall embodied carbon can be achieved by utilizing foundations with efficient geometry. By applying the parametric workflow systematically, insights are gained regarding shells' applicability to various building typologies and site conditions. Foundations are then considered within the context of a whole building to determine the potential downstream savings

✉ Kiley Feickert
feickert@mit.edu

[1] Department of Architecture, Massachusetts Institute of Technology, 77 Massachusetts Avenue, Cambridge, MA 02139, USA

Published online: 04 November 2023

when multiple structural elements are optimized to minimize material use and mass.

Shells are materially efficient due to their geometry. However, their complex curvature has hindered their implementation in contexts where skilled labor costs outweigh material costs, particularly in the Global North. Digital fabrication offers a pathway to economically build materially efficient foundations as innovations have led to increased productivity and reduced cost for construction applications, particularly for complex elements [5]. In this paper, robotically milled earth is proposed as a fabrication medium to cost effectively manufacture thin shell concrete foundations while minimizing the embodied carbon of formwork.

Environmental impact of reinforced concrete structural elements

Reinforced concrete (RC) structures are composite systems comprised of a large volume of reinforcing steel and concrete. Due to the processes required to manufacture them, both steel and concrete have a high ecological impact in terms of their carbon emissions and their consumption of nonrenewable resources. Construction accounts for over half the world's steel consumption [6] and cement production alone contributed approximately 8% of anthropogenic CO_2 emissions in 2012 [7]. Architects and engineers are pursuing many approaches to reduce emissions including material substitution and material reduction [8]. However, foundations are particularly challenging to build in materials other than RC. Additionally, RC has and will continue to be a key component in the sovereign development of countries around the world [9] and, therefore, should not be ruled out as a building material in all contexts. This suggests that developing methods for using less RC initially will be a key component in reducing building sector carbon emissions [10].

In this paper, *embodied carbon* (CO_2e) refers to the environmental impact of Cradle to Gate processes during Life Cycle Assessment (LCA) stages A1-A3 according to EN 15978:2011 (See Sec. 3.1). Emissions from extracting and transporting raw materials and manufacturing building materials are included, while emissions associated with transporting them to site and construction (LCA stage A4-5) as well as use stage (LCA stage B) are omitted. This paper focuses on stages A1-A3 due to the anticipated difference in material consumption for the respective foundation typologies, the specificity of the materials studied (concrete and reinforcing steel), and the reliability of embodied carbon values for these materials [11]. Additionally, over 90% of emissions for in-situ and prefabricated elements are attributed to LCA stages A1-A3 [12]. For this work, *embodied carbon* and *global warming potential* are used interchangeably.

Reinforced concrete structural elements, specifically the floor system, frame, and foundations, are the biggest contributors to embodied carbon in a building [13] for two reasons: 1) most of these elements work in bending, which is an inefficient method of load transfer requiring additional material to satisfy the design loads, and 2) prismatic elements (rather than elements with varying cross section responsive to nonuniform internal force demands) are built for ease of construction in contexts where labor costs outweigh material costs.

However, by utilizing RC only where it's required structurally, architects and engineers have demonstrated that significant material and carbon savings can be achieved. Different approaches include optimizing the shape of a one-way RC floor slabs [14], utilizing thin concrete vaulted floors [15, 16], and shape-optimizing beams [17]. Most research to date on structural optimization for embodied carbon minimization has focused on visible structural elements. However, foundations are a highly impactful and often overlooked contributor to embodied carbon in buildings and thus should also be studied for their potential to reduce carbon emissions.

Embodied carbon of foundations

Existing embodied carbon databases that quantify the environmental impact of foundations are summarized in Table 1.

The majority of studies are based on material take-offs from built projects [4, 18, 20, 21], while two utilize bottom-up structural design [3, 19]. In all analyses, only typical foundation typologies are evaluated (including spread footings, rafts, and piles). This literature provides a valuable baseline to understand the significance of foundations' contribution to carbon emissions, accounting for up to 42% of a structure's embodied carbon, on average. However, the large range in values (42–7%) can be attributed to the lack of data on geology, allowable settlement, and foundation typology, as well as different methods for collection, different building types, and the inclusion of different scopes (LCA Stage A1-D) for embodied carbon calculation. This lack of standardization limits the ability to analyze what is contributing to the material intensity of these foundations as well as which parameters they're most sensitive to. However, this limitation also offers an opportunity to study alternative foundation typologies utilizing bottom-up physics-based calculations to determine their environmental impact.

Literature review and background

There are several areas of existing work that relate to computational design optimization of foundations and efficient foundation typologies. This section reviews them and presents the research gaps identified by this paper.

Table 1 Non-exhaustive list of structural embodied carbon benchmarks that include mean embodied carbon contribution from foundations

Database / Publication	Method of collection	Structural elements included	LCA stages included	Building program	# of buildings/ samples	Mean EC contribution (%)
Carbon Leadership Forum Database [4]	Voluntary reporting of material takeoffs for built projects	Superstructure, foundations	Varies (A1-D)	Education, healthcare, mixed, multi-family, office, other, public assembly	557	42%
DeQo Database [18]	Voluntary reporting of material takeoffs for med-large scale, built projects	Foundations	A1-A3	Commercial, data centers, education, healthcare, hospitality, residential	200	27%
Gauch et al. [19]	Bottom-up structural design	Foundations	A1-A5	Office	3000	22%
Thornton Tomasetti Database [20]	Beacon; Revit material takeoffs	Foundations	Not reported	Educational	600+ across all programs	23%
				Residential		19%
				Commercial		17%
Kaethner and Burridge [3]	Bottom-up structural design	Substructure	A1-A4	Office	8	17%
				Hospital	6	11%
				School	6	11%
EU-ECB Database (France) [21]	Voluntary reporting of material takeoffs for built projects	Foundations, basement	Varies (A1-C4)	Not reported	486	7%

Foundation optimization

To date, foundation shape optimization has focused on a strict design space, limited to prismatic elements [23, 24]. Although insights are gained regarding the optimal shape of the spread footing typology, marginal embodied carbon savings are achieved. For example, when a multi-objective optimization is performed for average cost and average emissions, 7% (100 kg) CO_2e can be saved across 1000 designs [23]. This is because the optimization does not change the fundamental behavior of how the material is carrying the load. By utilizing geometry that transfers a column load to the soil below more efficiently, additional material reduction can be achieved.

Additionally, there is a lack of academic literature on foundation design optimization, when compared to other structural elements. In a 2020 survey of peer-reviewed optimization publications for RC structural components, a total of 7 articles were found on foundations, compared to 152 for RC frame structures [25]. Yet, foundations contribute between 7 and 42% of a structural system's overall embodied energy [4, 21]; therefore, foundations are both highly impactful and relatively understudied.

Efficient or innovative foundations through geometry

Historic examples suggest that material, and therefore embodied carbon, savings can be achieved by optimizing the geometry of foundations. Thin, RC shells are studied due to their ability to distribute loads more efficiently through their cross-section, reducing the quantity of material required structurally. Shell foundations create a spatial system that distributes the applied column loads primarily by in-plane or membrane forces to the soil below (See Fig. 1b), rather than through bending (See Fig. 1a) [26, 27]. As concrete is utilized most efficiently in compression, a reduction in concrete thickness and steel reinforcement can be achieved if mainly compressive stresses are induced [28].

The first known modern example of an RC shell foundation was designed and constructed by Félix Candela and Carlos Recamier in Mexico City in 1953 [29, 30]. Since then, the design and engineering methodologies for shell foundations have been well established, with most literature published to date from India and Russia [28]. India is the only country with a building code devoted specifically to shell foundations (consisting of the conical and hypar types) which was authored by Nainan P. Kurian, the most prolific author on the topic, upon which this work is based.

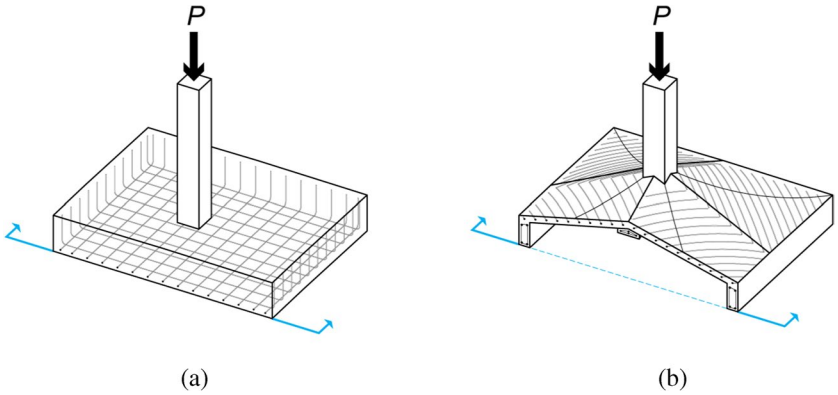

Fig. 1 For design load *P*, (**a**) typical spread footing, and (**b**) hypar shell footing

A historical review is beyond the scope of this paper, but a summary of previous investigations on shell foundations by the authors found that the most substantial cost reduction on a built project was 72% when a shell mat foundation was compared to a typical raft foundation for a factory building in Konnegar, India [30, 31]. The majority of built examples utilize shells due to the opportunity to save cost by reducing material consumption. This is typical in contexts where material costs outweigh labor costs, predominantly in the Global South. Shell foundations are therefore relatively understudied outside of this context.

Significant literature on the theory and application of shell foundation engineering exists for a multitude of pure shell forms. However, the environmental impact of their deployment has not been quantified. Due to their ability to substantially reduce material consumption, these precedents provide motivation for revisiting shell foundations to determine the quantity of embodied carbon that can be saved by utilizing efficient geometry.

Digital fabrication using earth

In contexts where labor costs drive construction costs, particularly in the Global North, elements that require more time to build are often overlooked due to perceived expense. However, if a significant reduction in embodied carbon can be achieved by building structural elements that are more complex, the building industry is urged to confront the challenges to fabricate them. Fortunately, innovations in digital fabrication have led to increased productivity and reduced cost for construction applications [5]. Therefore, contemporary digital fabrication techniques such as 3D printing or milling earth offer an economical pathway to achieving more complex structural elements while reducing carbon emissions.

Earth as formwork is a familiar concept in shell design and fabrication as demonstrated by Isler and Candela beginning in the 1950's [29, 32]. Advances in large scale additive manufacturing hardware and software also demonstrate that 3D printing local earth can be achieved at building scale [33, 34]. By utilizing this approach for foundations, the formwork can stay in place, which offers an opportunity for low cost, low carbon and no waste formwork, further reducing emissions. One opportunity is to 3D print earth into the shape required to receive an RC shell foundation. However, due to the requirement for foundations to transfer the loads of the building to the soil below, compacting the printed shape while maintaining the complex geometry requires further study.

Subtractive CNC milling for complex formwork is an alternative approach. This method typically relies on carbon intensive materials such as high-density foam. Alternatively, recyclable materials, such as frozen sand and ice, have been deployed successfully as formwork for concrete elements [35–37]. However, in these cases, the environmental control of the experiment was critical to its success. Additionally, topographical interventions have been studied at building scale using an autonomous excavator [38]. The final formations were not tested for their ability to transfer structural loads; however, much can be learned from these experiments for load-bearing applications.

Research gap and research questions

Materially efficient alternatives to existing building systems are necessary to explore to limit global warming while providing adequate housing for the increasing global population. Due to the lack of standardization across current reporting methods, there is an opportunity to quantify the environmental impact of foundations for various loading conditions and soil types to understand their relative carbon contribution using bottom-up physics-based calculations, rather than top-down material take-offs. Computational design is proposed to quickly iterate though these conditions and to create generalizable data. Additionally, there is an opportunity to explore alternative typologies and subtractive digital fabrication methods for structural applications where limited control on climate is expected, specifically for on-site fabrication in heat stressed regions.

The research questions that are central to this work are:

- To what extent can efficient geometry reduce carbon emissions in foundations?
- Can we leverage digital fabrication to construct complex geometry, if warranted by carbon savings?

To answer these questions, this research quantifies the environmental impact of business-as-usual foundation design by deploying a computational workflow to design spread and shell footings (Sec. 4.1.1), evaluates the applicability of shell foundations to various building typologies and contexts based on their carbon saving potential (Sec. 4.1.2), quantifies the downstream global warming potential saving when multiple structural elements utilize efficient geometry to transfer structural loads (Sec. 4.2), and investigates opportunities to construct shell footings by compacting local earth and then robotically milling it to act as formwork (Sec. 5.3).

Methodology

To evaluate the environmental impact of shell foundations compared to prismatic (spread) foundations, the methodology in Fig. 2 is used.

Embodied carbon comparison of shell and spread foundations

Conceptual overview

Existing physics-based analytical equations that design and size steel and concrete elements for shell and spread foundations are parameterized in a computational workflow for two reasons; 1) to understand the concrete and steel reinforcement material takeoffs of a given design in order to calculate the resulting embodied carbon, and 2) to quickly iterate through various structural and geotechnical conditions to output generalized data to understand the applicability of shell and spread footings to various contexts.

Due to the fact that the only known building code for shell foundations is from India, this research references the National Building Code (NBC) of India for structural mechanics, specifically the Indian Standard 456–2000: Plain and Reinforced Concrete Code of Practice (IS 456) [39]. This code can be compared to American Concrete Institute Code 318–19 (Building Code Requirements for Structural Concrete and Commentary), but is more conservative in some regards [14].

This research studies how changes in the factored column load ($P = 1$—5MN) and allowable soil bearing capacity ($q = 72$—575kN/m2) impact the overall carbon emissions of RC shell and spread footings. The range of soil load bearing

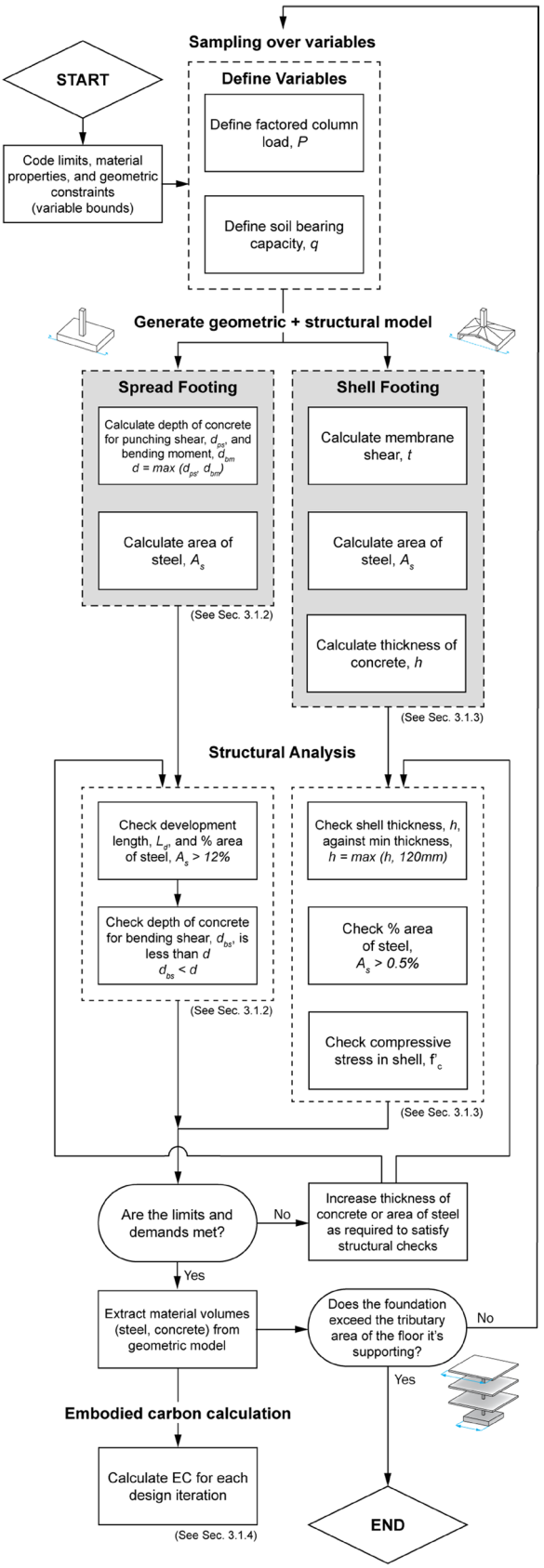

Fig. 2 Methodology for structural design and embodied carbon comparison of spread and shell footings

Table 2 Material properties for structural design and embodied carbon calculation * [22]

Material	Embodied Carbon Coefficient* ($kgCO_2e/kg$)	Density (kg/m^3)	Strength σ (MPa)
Plain concrete	0.15	2323	23
Steel, Rebar	1.99	7849	415

capacities, q, are extracted from Sect. 1806, Presumptive Load-Bearing Values of Soils, of the International Building Code [40]. Limits imposed by the NBC, material properties and geometric constraints are coded into a parametric workflow.

It performs the required structural checks by code and determines if those limits are met. If the limits are met, the material volumes are extracted for the respective designs to calculate embodied carbon.

A process-based LCA analysis for estimating embodied carbon is used due to the specificity of materials studied and the reliability of values for these materials [11]. The embodied carbon coefficients, or cradle-to-gate material coefficients, refer to the environmental impact of LCA stages A1-A3 according to EN 15978:2011 and come from the Inventory of Carbon and Energy database (Version 3, 2019) [22] (See Table 2).

This research focuses specifically on the embodied carbon impact of shallow foundations, given their ubiquity and compatibility with algorithmic analysis (in contrast with deep foundations, which require more site-specific information to engineer and obtain material quantities with specificity). While it's possible to use advanced numerical techniques such as form-finding or shape optimization to generate the shell geometry, a hyperbolic paraboloid (hypar) is used due to the extensive literature that's been published on its structural and geotechnical performance and its ability to save a significant quantity of material in published historic examples [28, 29]. Additionally, hypars have a square footprint and are ruled surfaces, which have benefits from a construction perspective, particularly for supporting high loads in a typical structural grid and incorporating reinforcing steel.

The workflow assumes that a column transfers the load of the building axially to an aligned footing, located in the center of a tributary area of $81m^2$. The geometry of the foundation is constrained by the tributary area so as to prevent overlap as the structural grid expands. It should be noted that in typical foundation design, when the area of individual spread footings exceeds 50% of the building footprint, a typological shift typically occurs, and mat foundations replace individual footings. However, in this research, the minimum material required to support the design load is being calculated until the geometric constraint is reached. This means that the embodied carbon values shown are likely more conservative than the values that would result from current construction processes.

The resulting structural design and embodied carbon values for a set of inputs in the parametric workflow are shown in Fig. 3.

Structural design of spread footings

The structural design for spread footings follows the design procedures outlined in *Design of Foundation Systems* [41]. These methods follow the Indian Building Code and are used to ensure the fairest comparison with the shell foundation engineering calculations, presented in the following section. The key dimensions are described by Fig. 4a and the section is shown in Fig. 4b.

Firstly, the bearing area of the spread footing is calculated by dividing the column load, P, by the bearing capacity of the soil, q, (Eq. 1). To calculate the area of steel and thickness of concrete for the spread footing, the column load, P,

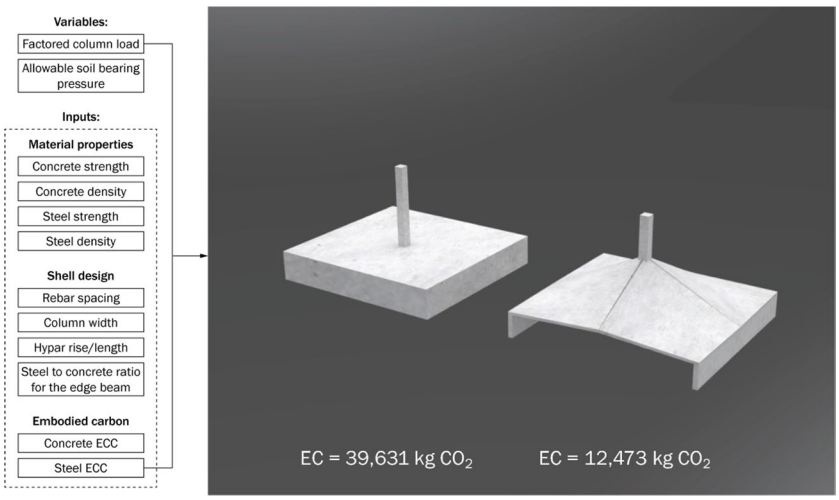

Fig. 3 Inputs for parametric workflow and resulting design and embodied carbon values for spread and shell foundations

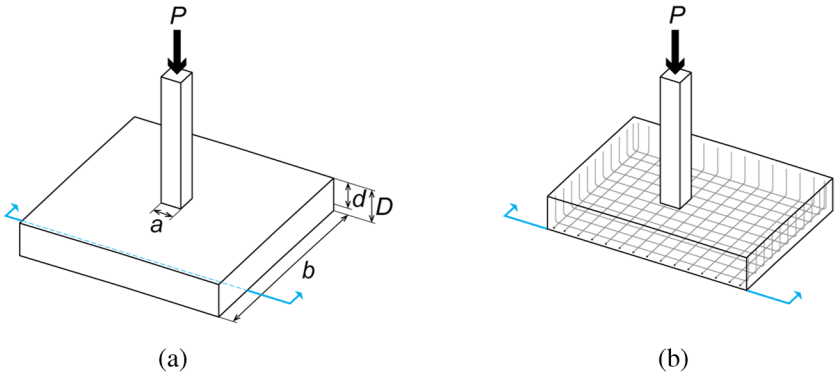

Fig. 4 (**a**) Dimensions of spread footing, and (**b**) section of spread footing

is first multiplied by a factor to safety (1.5) to get the factored design load, P_u. After calculating the design punching shear strength, τ_c, using Eq. (2), the depth of the footing, d_{ps}, is calculated by setting the total shear force on the critical section equal to the total resistance of the section in punching shear (Eq. 3), and solving for d_{ps} (Eq. 4).

$$b^2 = P/q \tag{1}$$

$$\tau_c = 0.25\sqrt{f'_c} \tag{2}$$

$$P_u[b^2 - (a + d_{ps})^2] = 4\tau_c(a + d_{ps})d_{ps} \tag{3}$$

$$d_{ps} = b\left[\left(-A_1 + (A_2 - A_3)^{0.5}\right)/A_4\right]A_1 = \left(\frac{a}{b}\right)\left[\left(\frac{P_u}{\tau_c}\right) + 2\right]A_2 = \left(\frac{a}{b}\right)^2\left[\left(\frac{P_u}{\tau_c}\right) + 2\right]^2 A_3 = \left[\left(\frac{P_u}{\tau_c}\right) + 4\right]\left(\frac{P_u}{\tau_c}\right)\left[\left(\frac{a}{b}\right)^2 - 1\right]A_4 = \left(\frac{P_u}{\tau_c}\right) + 4 \tag{4}$$

Next, the ultimate bending limit, M_u, is calculated using Eq. (5). This value is set equal to Eq. (6), the moment resistance of a balanced section of reinforced concrete, to ensure the section is not over-reinforced, which could result in the section failing by crushing in the concrete before steel reaches yield. The neutral axis in a singly reinforced concrete section is located at a depth, x_{umax}, with the centerline of the reinforcing steel located at a depth, d. The value, $\frac{x_{umax}}{d}$, depends on the strength of steel (see Table 2). In this case, $\frac{x_{umax}}{d} = 0.479$. Equation (7) is then used to find the depth, d_{bm}, required for bending moment.

$$M_u = (P_u/2)((b - a)/2)^2 \tag{5}$$

$$M_u = [0.36\left(\frac{x_{umax}}{d}\right)\left(1 - 0.42\frac{x_{umax}}{d}\right)f'_c]bd^2 \tag{6}$$

$$d_{bm} = \left(\frac{M_u}{\left[0.36\left(\frac{x_{umax}}{d}\right)\right]\left[1 - 0.42\left(\frac{x_{umax}}{d}\right)\right][f'_c * 1]}\right)^{0.5} \tag{7}$$

The higher value is taken from the depths calculated for punching shear, d_{ps}, and bending moment, d_{bm}, (Eq. 8) to design the area of steel, A_s. The depth for punching shear is typically greater than the depth for bending moment in the cases considered in this paper and is calculated to provide sufficient thickness to avoid shear reinforcement. No reinforcement is specified for the top layer of the footing, as it does not experience bending. Once the depth is defined, the area of steel, A_s, can be calculated using Eq. (9).

$$d = \max(d_{ps}, d_{bm}) \tag{8}$$

$$M_u = 0.87\sigma_{st}A_s d\left(1 - \frac{A_s\sigma_{st}}{bdf'_c}\right) \tag{9}$$

A rebar diameter is selected, ∅, and Eq. (10) is used to calculate development length. Design bond strength, τ_{bd}, is prescribed by Cl. 26.2.1.1 in the Code [39] and is multiplied by 1.6 for deformed bars in tension. The length of rebar is then checked to make sure it satisfies the development length using straight bars and subtracting for concrete cover, *cov*, using Eq. (11). A minimum cover of 50 mm is required on all sides of the spread footing, per Cl. 26.4.2.2.

$$L_d = \varnothing\sigma_{st}/4 * 1.6\tau_{bd} \tag{10}$$

$$L_d > \left(\frac{b - a}{2}\right) - cov \tag{11}$$

The percentage area of steel is checked against a minimum of 12% [C1:Cl.26.5.2.1] and then the section is checked to make sure it is not over-reinforced using Eq. (12).

$$\frac{0.87\sigma_{st}A_s}{0.36f'_c bd} < \frac{x_{umax}}{d} \tag{12}$$

As a check, the depth required to resist bending shear, d_{bs}, is determined using Eq. (13), where the design strength of concrete, τ_c, is prescribed by Code [39].

$$d_{bs} = (P_u(b - \frac{a+2d}{2}))/\tau_c \tag{13}$$

The calculated value of d_{bs} is checked to ensure it is less than the maximum depth obtained from Eq. (7). If the depth for bending shear is greater than the depth from 7, the depth must be revised to satisfy bending shear.

For this study, within the geometric constraints of the spread footing, the two structural checks that are not always met are; 1) that the development length of the rebar is greater than the width of the footing minus sufficient cover, and 2) that the depth calculated for bending shear is greater than the depth calculated for punching shear and bending moment. For the development length, the initial design assumes that rebar remains straight and is not turned up at the edge, due to the added complexity of maintaining it in position while concrete is poured. However, if sufficient development length is not achieved, it is assumed that the bars will be bent or hooked to achieve sufficient length. This occurs only within a small number of combinations, at low applied loads (0-1MN). To address the necessary depth to resist bending shear, thickness is added incrementally until all structural checks are satisfied for the given load case.

In parallel, a hyperbolic paraboloid (hypar) shell footing is designed for the same inputs as the spread footing.

Structural design of hyperbolic paraboloid shell footings

The structural design for a hypar shell footing is completed following design procedures outlined in Kurian's textbook, *Shell Foundations: Geometry, Analysis, Design and Construction* [28]. The shell membrane, edge beams and ridge beams are designed for simplified load cases. Uniform thicknesses are maintained, in line with Kurian's example, to be conservative. The rebar is designed to follow the curving lines of principal tension, as the quantity of steel can be reduced by half when compared to designing rebar to follow the straight-line generators [28]. The key dimensions and forces are described by Fig. 5a and b.

Hyperbolic paraboloid shells are investigated due to their geometry. They are comprised of doubly curved, anticlastic quadrants that can be constructed using straight line generators in either direction. This means hypars are both stiff and more easily fabricated than other shell typologies. They have also been deployed in applications throughout the world, as demonstrated by Félix Candela's examples in Mexico (See Sec. 2.2).

The bearing area of the shell is calculated the same way as Eq. (1) by dividing the column load, P, by the bearing capacity of the soil, q, (Eq. 14). To calculate the area of steel and thickness of concrete for the shell, the column load, P, is first multiplied by a factor to safety (1.5) to get the factored design load, P_u. The membrane shear, t, is a function of the geometry of the shell. For a hyperbolic paraboloid, the warp, k, is calculated using Eq. (15), and the membrane shear is then calculated using Eq. (16).

$$4a^2 = P/q \tag{14}$$

$$k = f/a^2 \tag{15}$$

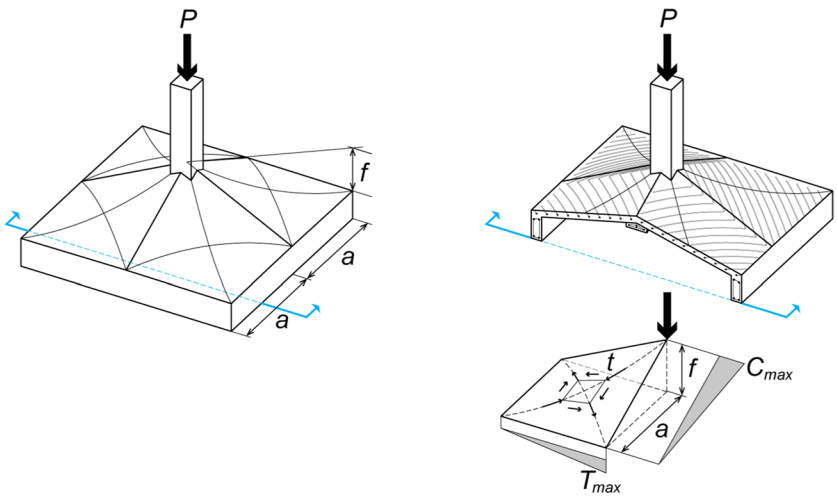

Fig. 5 (**a**) Dimensions of shell footing, and (**b**) section of shell footing with forces

Table 3 Geometric and material properties for ridge beam calculations [28]

Steel to concrete ratio,γ	Column width, c (m)	Rebar spacing (m)
0.05	0.4	0.15

$$t = P_u/2k \tag{16}$$

To calculate area of steel by strength, a safety factor (0.87) and the following Eq. is used:

$$A_s = t/(0.87\sigma_{st}) \tag{17}$$

The thickness of the shell, h, can then be calculated using:

$$m = 280/(3\sigma_c) \tag{18}$$

$$h = (t/1.5)/(0.14f'_c - (m-1)A_s) \tag{19}$$

Once the concrete thickness h is calculated, it is checked against a minimum thickness. If $h < 120mm$, 120 mm is used, as prescribed by code. The percentage area of steel is checked against a minimum of 0.5% and then the compressive stress in concrete ignoring steel is checked against the compressive stress in the equivalent section in the perpendicular direction using Eq. (20). In the cases studied for this paper, this condition is always met.

$$(t/1.5)/120 < (0.4f'_c)/1.5 \tag{20}$$

The area of steel in the edge beam is calculated to satisfy the maximum tension (located at the center of the beam) using Eq. (21). The height and width of the edge beam can then be found using Eq. (22).

$$A_{seb} = 2t/(0.87\sigma_{st}) \tag{21}$$

$$h_{eb} = \sqrt{(2t}/1.5)/(m-(m-1)A_{seb}) \tag{22}$$

Geometry of the ridge beam is designed following the steps outlined in Kurian's Sect. 6.4 [28]. Some geometric parameters are variable, such as the column width and rebar spacing, and are included as inputs into the parametric workflow. The values used for the following experiments are outlined in Table 3.

The area of concrete in the ridge beam is calculated using Eq. (23), and the area of steel in the ridge beam is calculated using Eq. (24).

$$A_{crb} = (2t * \sqrt{(a^2 + f^2)})/(0.4f'_c - \rho_s * 0.4f'_c + \rho_s * 0.67\sigma_{st}) \tag{23}$$

$$A_{srb} = A_{crb} * \gamma \tag{24}$$

Embodied carbon calculation

The resulting structural designs from Sects. 3.1.2 and 3.1.3 are then used to calculate embodied carbon using the material properties in Table 2. The volume, V, of concrete and steel, respectively, are extracted from the workflow and multiplied by their density, ρ, and embodied carbon coefficient, ECC, to determine the total kg CO_2e for each of the elements (Eq. 25). It should be noted that the volume of steel is not subtracted from the volume of concrete, as the difference is deemed negligible for the following experiments.

$$EmbodiedCarbon = V * \rho * ECC \tag{25}$$

The resulting embodied carbon is evaluated for factored column loads that range from 1-5MN, with results highlighted for 2MN and 5MN loads. The equivalent number of floors for a 2MN and 5MN load in various superstructure materials for an office building with a 9 m span are highlighted in Table 4 [42].

Embodied carbon impact of foundations in full structural building model

The parametric workflow described in Sect. 3.1 is then linked to a larger full building structural model, that computes dimensions for RC structural members and incorporates shape-optimization results for embodied carbon minimization for the floors and beams by Ismail and Mueller [14]. Columns are designed to be moment-continuous, and the cross-section is efficiently selected from typical dimensions using Karamba 3D. The purpose of this study is to understand how shape-optimized structural elements can be used in combination to reduce the overall global

Table 4 Number of floors for a 2MN and 5MN column load for flat concrete, shape-optimized concrete, steel, and timber superstructures [42]

Superstructure	# floors for 2MN column load	# floors for 5MN column load
Flat RC two-way slab with RC frame	-	3
Shape-optimized RC one-way slab with RC frame	3	9
Composite steel deck and RC floor (steel deck) with steel frame	3	9
Cross-laminated timber (CLT) floor with timber glulam frame	11	24

Table 5 Values used for designing full structural building model to evaluate the carbon saving potential of shape-optimizing floors, beams, and foundations

# of Floors	Span	Live load (kN/m^2)	Superimposed dead load (kN/m^2)	Soil Bearing Capacity	Concrete Strength	ECC (concrete) (kgCO2e/kg)
6	10 m	2.4	0.8	72kN/m^2	40 MPa	0.2768*

*value taken from data in Table 6

warming potential (GWP) of an RC structural frame during the design stage of a project. The lateral load resisting system (LLRS) is not considered for this study, as is it assumed that lateral stiffness is not the controlling factor for the designs sampled [43]. The model is flexible and parametric, allowing designers to vary a range of inputs.

For this study, the full building model is designed as a typical mid-rise office building. The loads and material properties used for design are described in Table 5. The resulting column loads on the footings are 2.22MN for perimeter columns and 4.43MN for internal columns, allowing for comparison to the results presented in Sect. 4.1.

Since foundations are furthest downstream in a building's load path, their size can be reduced if the mass of structural elements upstream is reduced. By shape-optimizing floors, for example, a significant reduction to the column load being resolved by the foundations results in a reduction in overall embodied carbon. Factored column loads, P_u, are extracted from the larger building frame model and are used as inputs for the parametric workflow described in Sect. 3.1. Different combinations of shape-optimized floors and foundations are studied to understand their interaction and emissions reduction potential (Sect. 4.2.1).

A study to evaluate the impact of concrete strength and shape-optimization of structural elements on embodied carbon is also conducted (Sect. 4.2.2). For this study, a range of embodied carbon coefficients are used, as emissions vary with concrete strength. A linear regression is used to approximate the embodied carbon coefficients of reinforced concrete based on strength for the self-reported Environmental Product Declarations for concrete in Mexico in the EC3 database (See Table 6) [44]. Mexico is chosen due to the high volume of concrete construction on low bearing capacity soils. A concrete strength of 40 MPa is taken as the baseline for the full building model design.

Table 6 Embodied carbon coefficient based on concrete strength for Mexico

Concrete Strength	Embodied Carbon Coefficient
20 MPa	0.1808
30 MPa	0.2288
40 MPa	0.2768
50 MPa	0.3248
60 MPa	0.3728

Results

The following experiments utilize the parametric workflow outlined in Sect. 3 to size steel and concrete in foundations to determine a shells ability to save embodied carbon through efficient geometry.

Single element comparisons

The design of foundations is highly specific to the load being imposed by the building above and the underlying soil strata. Various combinations are highlighted below.

Embodied carbon comparison of spread footings versus shell footings

Figures 6 and 7 present the embodied carbon quantification of spread and shell footings for two soil types and varying column loads. For clay soil ($q = 72$kN/m^2), hyperbolic paraboloid shells save a significant amount of embodied carbon when compared to a spread footing. For a 2MN load, the shell saves 48% CO_2e of the spread foundation for the same applied column load and soil bearing capacity (4,122 kg CO_2e and 8,001 kg CO_2e, respectively) (See Fig. 6). As the applied column load increases, the performance also increases. For a 5MN load, the shell saves 63% of the carbon emissions of the spread footing (12,319 kg CO_2e and 32,887 kg CO_2e, respectively) (See Fig. 6). The footings reach the geometric constraint of their tributary area at a column load ~ 5MN in clay soils, ending the iterative design process for both typologies.

As the bearing capacity increases from clay to sand ($q = 96$kN/m^2), shells continue to outperform spread footings, although the extent of their savings is slightly reduced. For a 2MN load, the shell footing saves 39% CO_2e of the spread footing (3,612 kg CO_2e and 5,945 kg CO_2e, respectively) (See Fig. 7). For a 5MN load, the shell saves 56% of the carbon emissions of the spread footing (10,807 kg CO_2e and 24,502 kg CO_2e, respectively) (See Fig. 7). Although

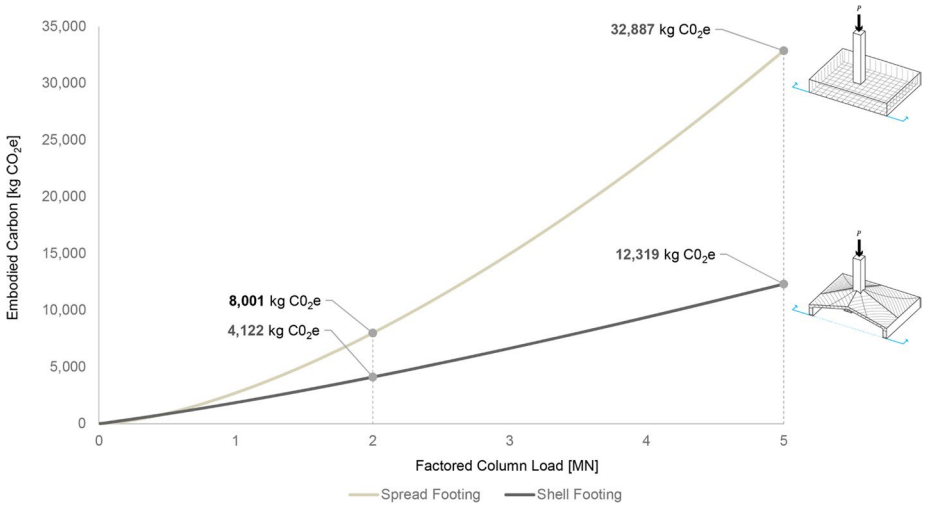

Fig. 6 Embodied carbon for spread footing and shell footing on clay soil ($q = 72\text{kN/m}^2$)

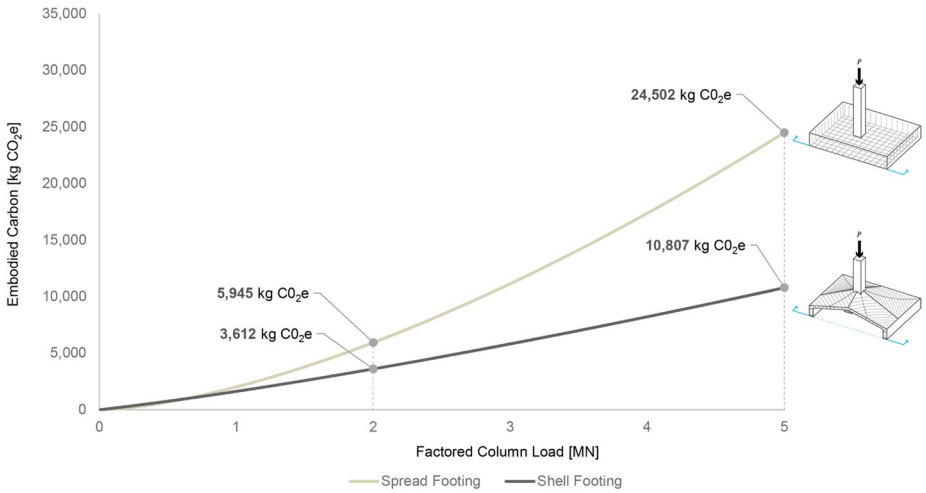

Fig. 7 Embodied carbon for spread footing and shell footing on sandy soil ($q = 96\text{kN/m}^2$)

the extent of the savings is reduced from clay soils, they are still substantial and warrant exploration to determine how to construct them.

This study is extended to all soil types in Sect. 4.1.2.

Applicability of shells to various contexts

Bearing capacities ranging from clay ($q = 72\text{kN/m}^2$) to bedrock ($q = 575\text{kN/m}^2$) and building loads ranging from 1 to 5MN are iterated through to create generalized data for the total embodied carbon of both a spread footing (Fig. 8) and a shell footing (Fig. 9). This study allows one to compare the relative environmental performance of the same foundation typology for a given column load and soil type.

For the spread footing, a large range of embodied carbon values can be seen (Fig. 8). This is due to the fact that spread footings require that the area of the foundation is large enough to spread the load of the building to the soil below, but also that they are sufficiently thick to resist bending, which is an inefficient method of load transfer. As the column load increases in low bearing capacity soil, the amount of material required to resist bending increases substantially, accounting for 32,887 kg CO_2e for a 5MN column load. Therefore, spread footings are particularly inefficient for this application.

The design space for shell footings is much flatter than spread footings, meaning they perform similarly in a range of soil types (Fig. 9). This makes their performance particularly advantageous in low bearing capacity soils (sand, clay, gravel), as opposed to the spread footing, which requires a significant amount of material and results in large quantities of carbon. However, for high bearing capacity soils (bedrock), spread footings outperform shells (See Tables 7 and 8). This is explored in more detail in Fig. 10.

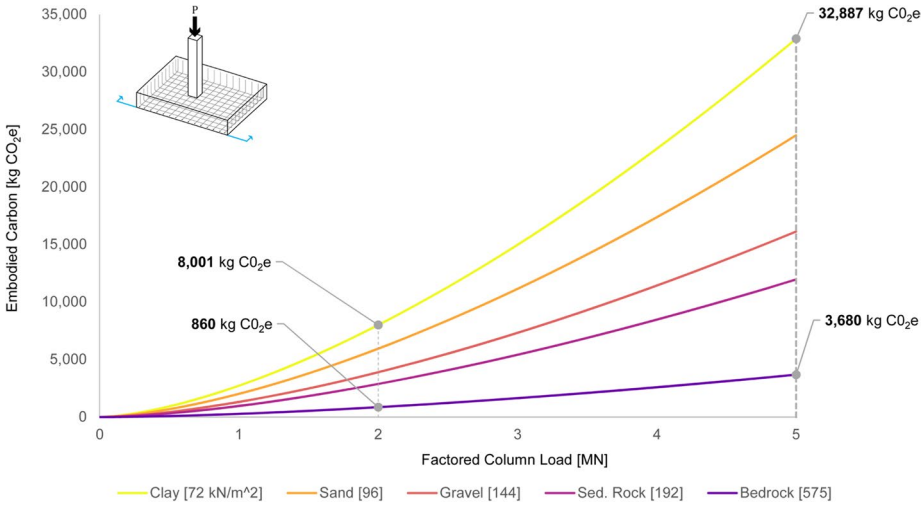

Fig. 8 Impact of column load on embodied carbon for spread footings for a range of soil bearing capacities

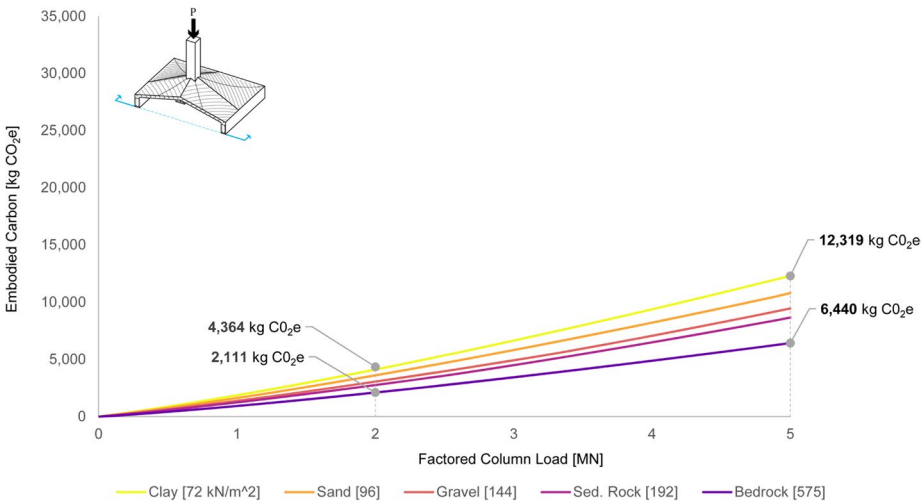

Fig. 9 Impact of column load on embodied carbon for shell footings for a range of soil bearing capacities

Table 7 Total embodied carbon for spread and shell footings in various soils for 2MN load

Foundation Typology	Total EC, Clay ($kgCO_2e$)	Total EC, Sand ($kgCO_2e$)	Total EC, Gravel ($kgCO_2e$)	Total EC, Sed. Rock ($kgCO_2e$)	Total EC, Bedrock ($kgCO_2e$)
Spread	8,001	5,945	3,896	2,876	860
Shell	4,122	3,612	3,062	2,762	2111
% change of total CO_2e from spread to shell	-48%	-39%	-21%	-4%	+46%

Table 8 Total embodied carbon for spread and shell footings in various soils for 5MN load

Foundation Typology	Total EC, Clay ($kgCO_2e$)	Total EC, Sand ($kgCO_2e$)	Total EC, Gravel ($kgCO_2e$)	Total EC, Sed. Rock ($kgCO_2e$)	Total EC, Bedrock ($kgCO_2e$)
Spread	32,887	24,502	16,134	11,961	3,680
Shell	12,319	10,807	9,468	8,666	6,440
% change of total CO_2e from spread to shell	-63%	-56%	-41%	-28%	+75%

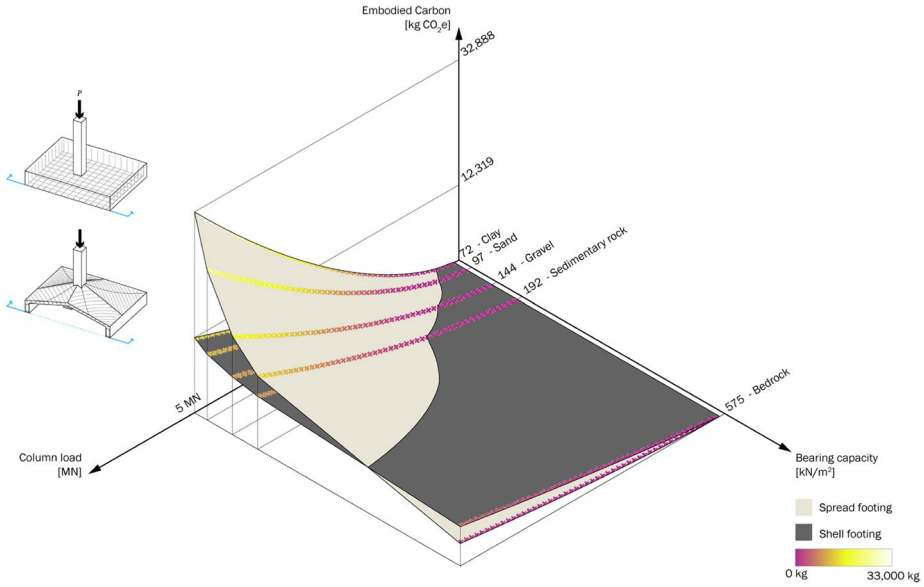

Fig. 10 Total EC contribution for spread and shell footings resulting from soil bearing capacity and column load

In order to compare the performance of the two typologies, the design space is visualized in 3 dimensions (See Fig. 10). Column load is shown on the x-axis [MN], soil bearing capacity is shown on the y-axis [kN/m^2], with the resulting embodied carbon shown on the z-axis [kg CO_2e]. It should be noted that this visualization represents the range of soil types that are present, not their prevalence. For example, it is rare to see bedrock present at the surface of site stratigraphy, and it is more common to see lower bearing capacity soils such as clay, sand and gravel. Therefore, one should focus on the embodied carbon saving potential of these lower bearing capacity soils as having broader potential applicability to many sites.

The significant savings that shells achieve for low bearing capacity soils and high applied column loads are prominent in Fig. 10. However, this is not always the case. Spread footings outperform shells where the applied column load is low and in high bearing capacity soils, which is indicated by the gray surface being located above the tan surface.

This is attributed to two findings; 1) that the minimum concrete cover for reinforcement in shells results in a thickness much greater than the thickness required to satisfy the structural demands, and 2) the added curvature of the shell for a small footprint increases total material quantities. To satisfy the structural design code, the minimum shell thickness is set at 120 mm to provide sufficient thickness for cover. In theory, however, the shell could be substantially thinner.

This suggests that alternative reinforcement can be explored, such as fibers or fabric, to reduce the thickness and total embodied carbon by removing steel in the shell surface entirely. Another opportunity to reduce embodied carbon in the shell is to shape-optimize the edge beam and ridge beam, which are currently designed as prismatic elements. As the tension of the edge beam is highest in the center of the shell edge and reduces to zero at the corner, the shape could be optimized to reflect this. Reinforcement continuity would be a challenge in this study but warrants further exploration. Shape optimization can also be applied to bending-dominated solutions, such as spread footings. If these prismatic elements are transformed to carry the building load more efficiently, material reduction can be achieved.

The environmental impact of concrete (Fig. 11) and steel (Fig. 12) to total embodied carbon is extracted from the study above to determine their respective contribution to the overall design. The total embodied carbon of both the shell and the spread footing comes almost entirely from concrete. This explains why the surfaces in Fig. 11 are very similar to those of Fig. 10. The quantity of concrete is more sensitive to applied loads than to bearing capacity, with the highest divergence between the shell and spread footing occurring at low bearing capacity soils. As the bearing capacity of the soil increases, the difference in concrete volumes and GWP between the shell and spread footing decreases significantly.

The volume of steel contributes much less to the overall embodied carbon of foundations than concrete (Fig. 12). Unlike floors, spread footings do not experience bending in the top layer of the concrete and, therefore, don't require steel there. In contrast to concrete, steel is more sensitive to the bearing capacity than to the applied load. For low bearing capacity soils, steel volumes are more comparable for spread and shell footings. However, as the bearing capacity of the soil increases to bedrock, shells require significantly more steel than spread footings, as spread footings experience minimum bending.

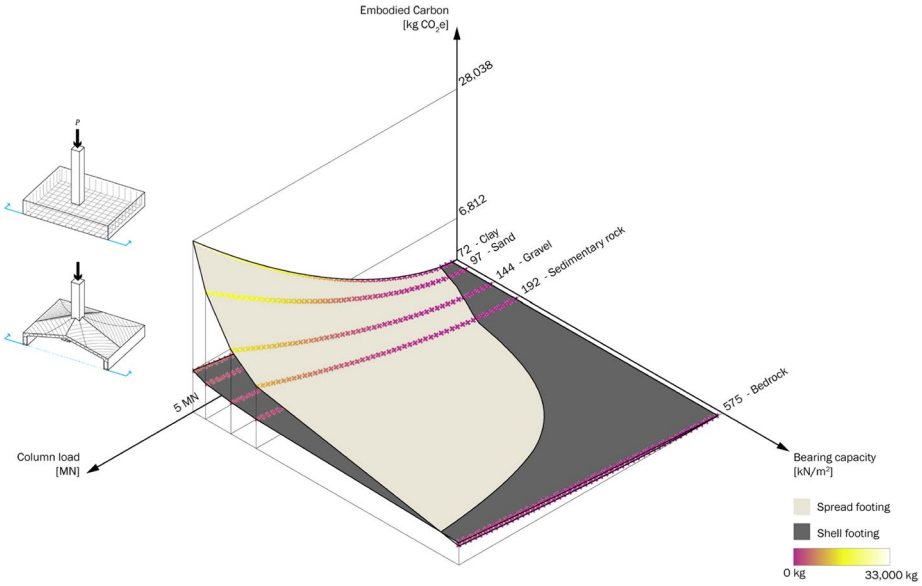

Fig. 11 Partial EC contribution from concrete for spread and shell footings resulting from soil bearing capacity and column load

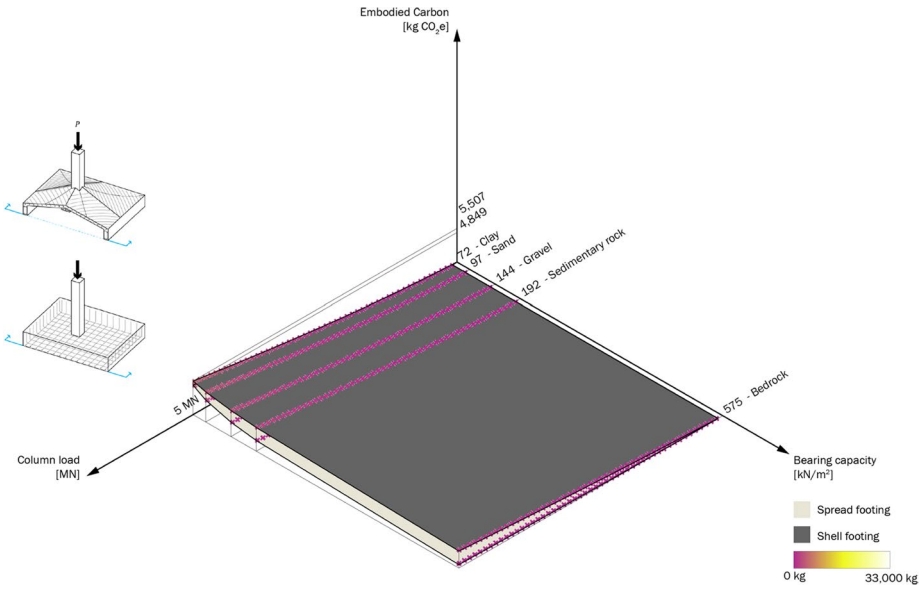

Fig. 12 Partial EC contribution from steel for spread and shell footings resulting from soil bearing capacity and column load

Full structural building model global warming potential reduction

The full structural building model analysis evaluates how geometrically efficient structural elements can be used in combination to reduce the overall GWP of an RC structural frame. In this study, floor slabs and foundations are designed using conventional methods and then optimized using efficient geometry to compare the environmental impact of these typological changes. Since a building's structural elements are interrelated, reducing the mass of upstream structural elements through optimization has a direct impact on the loads being resolved by the foundations. If large-scale material savings are desired to limit carbon emissions, structural systems must be considered holistically.

Impact of geometrically efficient floors and foundations on building frame GWP

The methodology in Sect. 3.2 is utilized to determine the reduction in GWP if various structural elements that typically work in bending utilize efficient geometry for clay soils ($q = 72\text{kN/m}^2$) (See Fig. 13). If the floor slabs are shape-optimized in isolation, a reduction in the structures

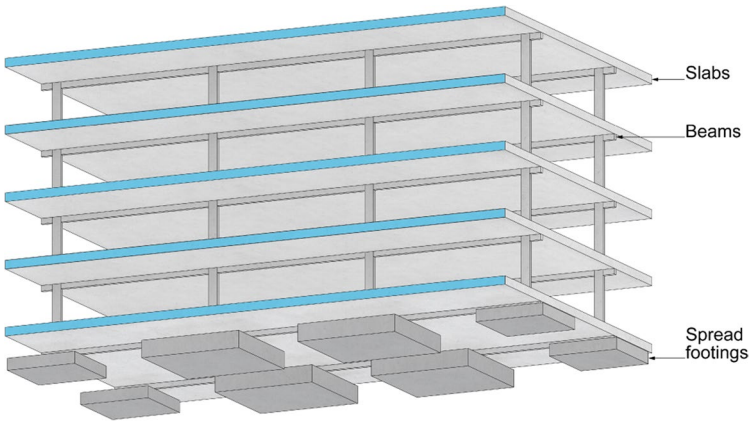

Fig. 13 Structural systems that typically work in bending include flat one-way spanning floor slabs, beams, and spread footings

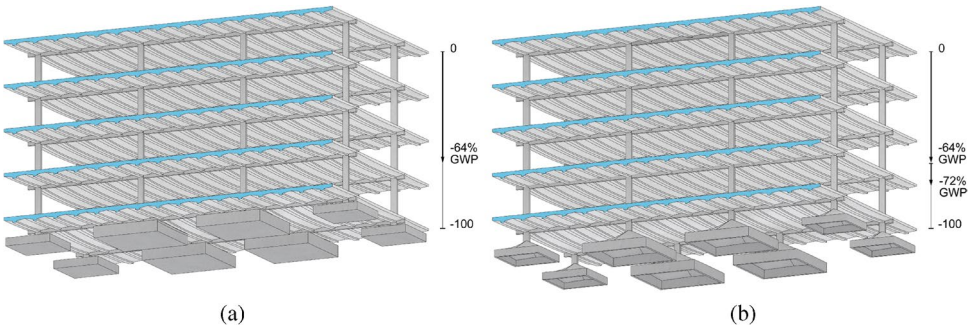

(a) (b)

Fig. 14 The savings in global warming potential of the structural frame when (**a**) floor slabs are optimized (64%), and (**b**) floor slabs are optimized and shell foundations are used (72%) for the conditions outlined in Sect. 3.2

GWP of 64% is achieved. By shape-optimizing only the beams, a reduction of 4% GWP is achieved and switching from spread to shell foundations saves 20% GWP.

Floor slabs contribute the majority of the embodied carbon of a building's upstream structural elements [45, 46]. As foundations are the last element in the load path, acting to resolve the weight of the building to the soil below, the demand on the foundations is reduced substantially if elements are optimized upstream. In isolation, switching from a spread footing to a shell footing on clay soil achieves a saving of 20% GWP (for the soil bearing capacity studied). However, if this switch is implemented in combination with shape-optimizing the floors, a total GWP reduction of 72% is possible, as floors contribute the majority of carbon emissions in the structural frame (See Fig. 14), and have the most potential to limit emissions. However, for high bearing capacity soils, such as sedimentary rock, no additional GWP saving is achieved if shell foundations are implemented for reasons described in Sect. 4.1.2.

Impact of concrete strength and geometrically efficient floors and foundations on building frame GWP

The impact of concrete strength is also studied to determine if additional carbon savings can be achieved when floors are shape-optimized and shell foundations are used (See Fig. 15). The same concrete strength is used for the structural frame, floors and foundations being designed for each scenario.

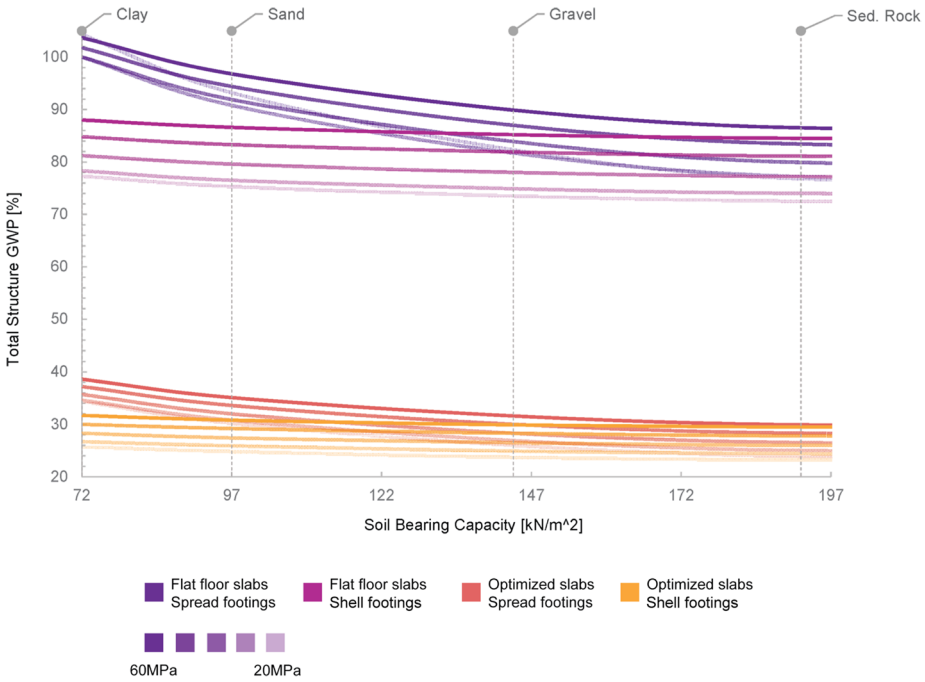

Fig. 15 In most cases, lower strength concrete is associated with lower total emissions for the respective combinations of optimized structural elements. As the soil bearing capacity increases, the benefit of utilizing optimized footings lessens. 100% GWP corresponds to the baseline design outlined in Table 5 with flat floor slabs and spread footings

Table 9 Impact of concrete strength on total structural frame global warming potential for clay soils for optimized floor slabs and foundations. *Baseline scenario used to calibrate model (See Sec. 3.2)

Concrete Strength	Embodied Carbon Coefficient	Flat floor slabs Spread footings (% GWP)	Flat floor slabs Opt. footings (% GWP)	Optimized slabs Spread footings (% GWP)	Optimized slabs Opt. footings (% GWP)
20 MPa	0.1808	104.3	77.3	34.4	25.7
30 MPa	0.2288	100	78.3	34.6	26.7
40 MPa	0.2768	100*	81.2	35.7	28.3
50 MPa	0.3248	101.8	84.8	37.2	30
60 MPa	0.3728	103.7	88	38.6	31.7

As expected, based on the results from Sect. 4.2.1, the most substantial GWP saving is achieved by shape-optimizing RC floors. By combining shape optimized floor slabs with shell foundations, ~ 72–79% reduction in total GWP for the structural frame can be achieve for clay soils, depending on concrete strength. In all scenarios (with the exception of flat floor slabs and spread footings for 20 MPa concrete), lower strength concrete is associated with lower total emissions for the respective combinations of optimized structural elements. Since the embodied carbon of concrete typically increases with strength for standard mix designs, any material reduction achieved by using higher strength concrete is offset by the increased emissions. This suggests that low strength and low embodied carbon materials may also be substituted for virgin concrete, further reducing shell foundations' total emissions. Additionally, utilizing shell foundations has the biggest impact in low bearing capacity soils, with only marginal savings achieved by implementing them in high bearing capacity soils (See Table 9).

In summary:

- The CO_2e saving potential of utilizing shell foundations in lieu of prismatic foundations depends largely on the soil bearing capacity as well as the optimization of structural systems further upstream.
- Concrete strength has a lesser, but notable impact on the saving potential of shell foundations.

(a) (b)

Fig. 16 (**a**) Filling timber formwork with adobe mixture, and (**b**) tamping adobe

Thin shell foundation prototype using digital fabrication

This paper demonstrates the potential for shell foundations to reduce embodied carbon significantly. However, a key question remains as to how to construct them in an economically competitive manner, given the relative geometric complexity compared to spread footings. This section proposes and evaluates a method for robotically milling compacted earth as in situ formwork to fabricate thin shell footings economically.

Robotically milled earth formwork for thin RC shells

The curvature and thinness that results in material savings in shell foundations also makes them more time-consuming to construct using traditional building methods when compared to prismatic elements. Taking inspiration from the application of digital fabrication to construct complex or nonstandard geometry, robotically milled earth, or adobe, is explored as formwork for the RC shells (Fig. 16).

Fabrication approach

The proposed fabrication method is experimentally tested on a 1:17.5 scale thin-shell footing prototype measuring 230 mm square in plan. A KUKA-brand six-axis industrial robot arm is used in conjunction with a ceramic metal loop end-effector for this experiment. A toolpath for the robot is programmed using the KUKA|prc (parametric robot control) plug-in for grasshopper. This toolpath successively removes layers of adobe from a flat plane to the doubly-curved hyperbolic paraboloid surface which acts as the formwork for the desired shell geometry. The KUKA traces back and forth across the adobe successively loosening material with the loop tool while a shop vacuum is simultaneously removing the loosened material until the

(a) (b)

Fig. 17 Robotic milling of adobe to act as formwork for thin concrete shell (**a**) roughing pass one, and (**b**) roughing pass three

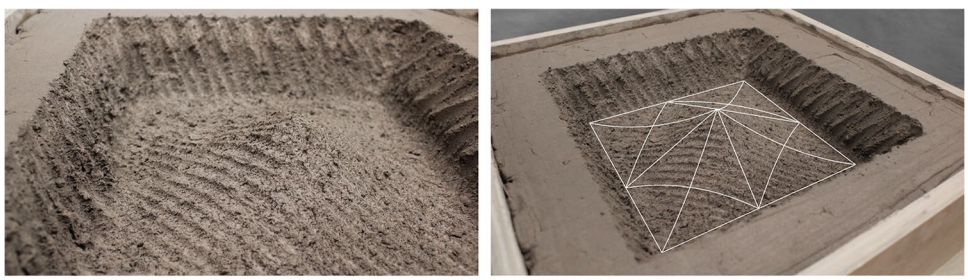

(a) (b)

Fig. 18 (**a**) Final adobe formwork for thin RC shell foundation prototype, with (**b**) linework overlaid to show curvature of surface

Fig. 19 (**a**) Vertical timber members added to perimeter of adobe formwork, and (**b**) thickness of first layer of concrete being checked with 3D printed template

Fig. 20 (**a**) Rebar added along principal stress lines, and (**b**) second layer of concrete applied to adobe formwork

final form is achieved. Roughing passes are used (Fig. 17) to remove the initial layers, then a finishing pass achieves the final formwork geometry (Fig. 18). A more uniform surface can be achieved by increasing the number of finishing passes at the expense of additional fabrication time. However, the bearing capacity of a shell has been shown to increase with an increase of roughness at the interface between the soil and shell [28], which is why a perfectly smooth surface was not desired. Concrete is then cast on the adobe formwork to create a thin shell foundation prototype (Figs. 19 and 20).

Various adobe mixes were tested for their ability to be easily milled while maintaining the desired formwork geometry. In this experiment an adobe mixture consisting of 42% clay, 42% sand, 16% water was used. Once the adobe is placed in the timber formwork (Fig. 16a), it is compacted using a tamp (Fig. 16b) to prepare it for milling. Future work will include performing a direct shear test on the adobe mixture to evaluate the strength parameters of the material to compare to local soils as well as fabricating a full-scale prototype to evaluate fabrication accuracy and to evaluate the environmental impact of the robotic processes, which has been shown to account for around 5% of a thin concrete shell floor system [47].

Following the fabrication of the formwork, concrete is cast on the adobe to create a thin shell foundation. First, timber formwork is added to the perimeter of the shell (Fig. 19a) and a layer of plastic is added to ensure the adobe does not remove moisture from the concrete as it's curing which may cause it to crack. As concrete is applied, the thickness is checked with a 3D printed template (Fig. 19b) to ensure uniform thickness. After the first layer of concrete is applied, reinforcing bars are evenly spaced with rebar chairs inserted into the clay to keep them in place (Fig. 20a). Concrete is then spread evenly on top of the reinforcing bars until the formwork is coated with an even thickness of concrete (Fig. 20b).

Fig. 21 (**a**) Side view of cured concrete shell foundation, and (**b**) cured concrete shell foundation on adobe formwork

Observations and results

The resulting thin concrete shell foundation (230 × 230 mm) can be seen in Fig. 21. Milling adobe effectively achieves the doubly-curved geometry required to construct a hyperbolic paraboloid shell, while allowing the formwork material to be compacted prior to fabricating the final form. This process can be scaled up using autonomous robots and larger scale end-effectors either to route or scrape the material into place in a similar manner as proposed here. Challenges that were experienced at this scale, such as creating rebar chairs for the reinforcement within a shell thickness of approximately 9.5 mm, are not necessarily applicable at building scale. However, challenges such as the potential for the adobe mixture to dry out the concrete during curing is also possible at full scale and needs to be considered. The surface roughness generated from the loop may also improve the shell/soil interface but requires further study.

Conclusion

The purpose of this paper is to identify and characterize the opportunities that shell foundations offer for mitigating the carbon emissions causing the climate crisis and to encourage architects and structural engineers to revisit shell foundations as a means to reduce material consumption in building structures.

Business-as-usual construction practices have led the building sector to contribute 13% of today's GHG emissions in the form of embodied carbon [2]. Foundations are an unseen source of carbon emissions in our buildings; however, if global warming is to be limited, we must consider their impact. This work demonstrates that by utilizing shell foundations, which take advantage of efficient geometry to transmit loads to the soil, material consumption and embodied carbon can be reduced substantially in specific contexts. Additionally, contemporary digital fabrication methods provide an opportunity to manufacture the complex curvature required for shell foundations in contexts where their implementation has been perceived as economically disadvantageous thus far.

Summary of contributions

The contributions of this research can be summarized as follows:

- This paper presents the first quantification and comparison of the environmental impact of typical spread footings and shell footings for a variety of building conditions across a range of soil types.
- In summary, hyperbolic paraboloid shell footings save a significant amount of embodied carbon when compared to spread footings in low bearing capacity soils, with the greatest CO_2e savings at high applied loads. In locations where bedrock is present, spread footings are the more materially and carbon efficient typology due to minimum concrete cover requirements for reinforcement and the added curvature of the shell. However, in the majority of cases studied, the CO_2e saving potential of utilizing shell foundations warrants consideration for implementation.
- The finding that the CO_2e saving potential of utilizing shell footings also depends largely on the optimization of structural systems further upstream. The GWP of a building's structural system can be reduced by nearly three-quarters when efficient foundation geometry is combined with shape-optimized floor slabs in low bearing capacity soils. Concrete strength has a lesser, but notable impact.
- This paper demonstrates an approach for constructing doubly curved concrete shells through an experimental prototype using robotically milled earth as formwork.

Potential impact

By promoting efficient geometry for structural elements, significant carbon savings can be achieved in rapidly urbanizing areas with weak soils. If deployed in isolation, shell footings have the potential to save almost half of the embodied carbon compared to typical spread footings for low rise or light-weight buildings (with a column load of approximately 2MN). As the height and/or weight of a building increases, (to a column load of approximately 5MN), the CO_2e saving potential also increases by up to two-thirds. If efficient geometry is utilized for both a building's floors and foundations, the same floor area can be built with one-quarter of the global warming potential of a structural system constructed using typical prismatic elements. As construction will necessarily increase to keep up with the growing global population, this significant reduction in carbon emissions allows for more floor area to be built, while substantially reducing the carbon emissions that would be incurred using business-as-usual construction methods.

This significant reduction in carbon emissions is possible today, however, has been inhibited by the complexity of the geometries and unfamiliarity of the typologies. Fabricating earth formwork for complex shell geometry using subtractive robotic milling provides a pathway to implement thin shell foundations in locations where labor costs typically outweigh material costs, in order to lessen the building industry's contribution to the climate crisis and ultimately, to limit global warming. Additionally, utilizing earth for formwork reduces the associated cost, material consumption, and emissions for the formwork, itself.

Limitations and future work

The work presented here evaluates isolated thin shell foundations against one typology of typical shallow foundations that work in bending, the spread footing. There is the potential to expand this investigation to other typologies, including friction piles, which do not work in bending. Additionally, the optimization of the shell shape through form-finding or evaluating other pure shell forms could lead to additional carbon savings in isolation or in a mat configuration and warrants further exploration. Reinforcement, such as reinforcing fibers or a reinforcing textile, that doesn't require substantial cover from concrete may greatly reduce total concrete consumption in the shell, further taking advantage of its efficient geometry. This also has the potential to extend the applicability of shells to higher bearing capacity soils and low column loads, where spread foundations currently outperform them. The interaction between multiple shells in a linear or mat arrangement could also provide additional structural and material reduction benefits. Additionally, this study can be extended to lower strength or reclaimed materials, which have the potential to further reduce emissions associated with foundations.

In practice today, design and engineering teams rely on site-specific stratification surveys provided by geotechnical engineers to engineer custom foundations for individual projects, rarely with consideration of carbon minimization strategies. Alternatively, on projects that don't require site-specific information, conservative assumptions are often used, resulting in overly material intensive solutions that incur significant economic and environmental costs. This work aims to establish a workflow that can be deployed to make data-driven assessments of where emissions savings can be achieved economically through shape optimization of foundations and other structural elements, depending on site conditions. Extending the full structural building model workflow to other superstructure materials and other spans would provide insight regarding the ideal spans for different contexts, as changing the span would affect optimization of the horizontal spanning elements as well as the column loads and number of columns. Including the LLRS would further strengthen the analysis, as it can account for around 13% of a structure's total embodied carbon in a low- to mid-rise building [48]. Therefore, identifying where materially efficient foundations and related technologies have the largest emissions saving potential by linking this workflow to site-specific geotechnical data is an opportunity to promote urban growth while reducing environmental impact.

Concluding remark

Since construction will necessarily continue at high rates to meet global demand, alternative building methods must be explored to limit carbon emissions in the building sector. By highlighting the costly environmental impact of foundations, this work seeks to encourage architects and engineers to more holistically understand and quantify the potential impact of our design choices. Substantial carbon savings are possible, today, using geometry that efficiently uses material only where structurally necessary. Although these forms are more complex than the geometries that are typically built, the potential to save a significant portion of a building's embodied carbon warrants their consideration. Thin shell foundations are especially relevant for buildings with high column loads and should be considered for deployment in rapidly densifying areas with weak soil.

Acknowledgements The authors are grateful to Dr. Nainan P. Kurian for his foundational work on this topic and for his support in the pursuit of this research. The authors would also like to thank Professor Sigrid Adriaenssens and Professor Andrew Whittle for generously sharing their comments, expertise and insights in structural and geotechnical engineering as this research was developed.

Funding 'Open Access funding provided by the MIT Libraries' Funding for this research was provided in part by the Dar Group Urban Seed Grant Program at the Norman B. Leventhal Center for Advanced Urbanism, Massachusetts Institute of Technology.

Declarations

Conflict of interest On behalf of all authors, the corresponding author states that there is no conflict of interest.

References

1. Gül T, Pales A, Levi P, Remme U, Teter J, Abergel T, Bains P, Bermudez Menendez J, Delmastro C, Gorner, M, Guoy A, Malischek R, Mandova H, Morgan T, Paoli L, Tattini J, Vass T (2020) Energy technology perspectives 2020. International Energy Agency/OECD
2. International Energy Agency (2022). "Buildings, IEA," Paris. [Online]. Available: https://www.iea.org/reports/buildings

3. Kaethner SC, Burridge JA (2012) Embodied CO2 of structural frames. Struct Eng 8
4. Simonen K, Rodriguez B, Barrera S, Huang M (2017) "Embodied carbon benchmark study: LCA for low carbon construction," Part One [Online]. Available: http://hdl.handle.net/1773/38017
5. García de Soto B, Agustí-Juan I, Hunhevicz J, Joss S, Graser K, Habert G, Adey BT (2018) Productivity of digital fabrication in construction: cost and time analysis of a robotically built wall. Autom Constr 92:297–311. https://doi.org/10.1016/j.autcon.2018.04.004
6. Allwood JM, Cullen JM (2015) Sustainable materials without the hot air: making buildings, vehicles & products efficiently and with less new material. UIT Cambridge Ltd
7. Miller SA, John VM, Pacca SA, Horvath A (2018) Carbon dioxide reduction potential in the global cement industry by 2050. Cem Concr Res 114:115–124. https://doi.org/10.1016/j.cemconres.2017.08.026
8. Fang D, Brown N, De Wolf C, Mueller C (2023) Reducing embodied carbon in structural systems: a review of early-stage design strategies. J Build Eng 76. https://doi.org/10.1016/j.jobe.2023.107054
9. Ismail M, Mueller C (2022) "Outrage: colonial legacies of concrete," Archit Rev. https://www.architectural-review.com/essays/outrage/outrage-colonial-legacies-of-concrete (accessed Apr. 16, 2022)
10. Fischedick M, Roy J, Abdel-Aziz A, Acquaye A, Allwood JM, Ceron J-P, Geng Y, Kheshgi H, Lanza A, Perczyk D, Price L, Santalla E, Sheinbaum C, Tanaka K (2014) Industry. In: Edenhofer O, Pichs-Madruga R, Sokona Y, Farahani E, Kadner S, Seyboth K, Adler A, Baum I, Brunner S, Eickemeier P, Kriemann B, Savolainen J, Schlömer S, von Stechow C, Zwickel T, Minx JC (eds) Climate change 2014: mitigation of climate change. Contribution of working group III to the fifth assessment report of the intergovernmental panel on climate change. Cambridge University Press, Cambridge and New York, NY
11. Weber RE, Mueller C, Reinhart C (2022) Solar exoskeletons – An integrated building system combining solar gain control with structural efficiency. Sol Energy 240:301–314. https://doi.org/10.1016/j.solener.2022.05.048
12. Wong F, Tang Y (2012) Comparative embodied carbon analysis of the prefabrication elements compared with in-situ elements in residential building development of Hong Kong. International Journal of Civil and Environmental Engineering.
13. Adams M, Burrows V, Richardson S (2019) Bringing embodied carbon upfront: coordinated action for the building and construction sector to tackle embodied carbon. World Green Building Council. https://worldgbc.org/article/bringing-embodied-carbon-upfront/
14. Ismail M, Mueller C (2021) Minimizing embodied energy of reinforced concrete floor systems in developing countries through shape optimization. Eng Struct 246:112955. https://doi.org/10.1016/j.engstruct.2021.112955
15. Hawkins W, Orr J, Ibell T, Shepherd P (2020) A design methodology to reduce the embodied carbon of concrete buildings using thin-shell floors. Eng Struct 207:110195. https://doi.org/10.1016/j.engstruct.2020.110195
16. López DL, Veenendaal D, Akbarzadeh M, Block P (2014) Prototype of an ultra-thin, concrete vaulted floor system. Proceedings of the IASS-SLTE 2014 Symposium 8
17. Orr J, Darby AP, Ibell T, Evernden MC, Otlet M (2011) "Concrete structures using fabric formwork," https://doi.org/10.17863/CAM.17019
18. Pratt, Q. (2016). Material quantities of foundation systems in building structures [Thesis, Massachusetts Institute of Technology] [Online]. Available: https://dspace.mit.edu/handle/1721.1/104234. Accessed 18 Nov 2020
19. Gauch HL, Hawkins W, Ibell T, Allwood JM, Dunant CF (2022) Carbon vs. cost option mapping: A tool for improving early-stage design decisions. Autom Constr 136:104178. https://doi.org/10.1016/j.autcon.2022.104178
20. Hattan A (2019) "Thornton Tomasetti Shares Results of Comprehensive Embodied Carbon Measurement Study | Thornton Tomasetti," https://www.thorntontomasetti.com/news/embodied-carbon-measurement-study (accessed Oct. 03, 2022)
21. Röck M et al (2022) "Towards embodied carbon benchmarks for buildings in Europe - #2 Setting the baseline: A bottom-up approach," Zenodo. https://doi.org/10.5281/ZENODO.5895051
22. Jones C, Hammond G (2019) "Inventory of Carbon & Energy (ICE)." Accessed: Jul. 12, 2019.[Online]. Available: http://www.circularecology.com/ice-database-faqs.html
23. Camp CV, Assadollahi A (2013) CO2and cost optimization of reinforced concrete footings using a hybrid big bang-big crunch algorithm. Struct Multidiscip Optim 48(2):411–426. https://doi.org/10.1007/s00158-013-0897-6
24. Wang Y, Kulhawy FH (2008) Economic design optimization of foundations. J Geotech Geoenvironmental Eng 134(8):1097–1105. https://doi.org/10.1061/(ASCE)1090-0241(2008)134:8(1097)
25. Afzal M, Liu Y, Cheng JCP, Gan VJL (2020) Reinforced concrete structural design optimization: A critical review. J Clean Prod 260:120623. https://doi.org/10.1016/j.jclepro.2020.120623
26. Das MK (1989) Three dimensional finite element model to study the behavior of hyperbolic paraboloid shell as foundation [Master of Science in Civil Engineering Thesis, Bangladesh University of Engineering and Technology]. http://lib.buet.ac.bd:8080/xmlui/handle/123456789/2540h
27. Williams C (2014) What is a shell? In: Adriaenssens S, Block P, Veenendaal D, Williams C (eds) Shell structures for architecture: form finding and optimization. Routledge/ Taylor & Francis Group
28. Kurian NP (2006) Shell foundations: geometry, analysis. Design and Construction, Alpha Science International Ltd
29. Candela F (1955) Structural Applications of Hyperbolic Paraboloidical Shells. ACI Struct J 51(1):397–416
30. Abdel-Rahman M (1996) Geotechnical behavior of shell foundations [Doctor of Philosophy Thesis, Department of Civil Engineering, Concordia University]. https://spectrum.library.concordia.ca/id/eprint/128/
31. Feickert K, Mueller CT (2021) Thin shell foundations: historical review and future opportunities. IASS Annual Symposium 2020/21. 7th International Conference on Spatial Structures, Guilford, UK
32. Moreyra Garlock ME, Billington DP (2014) Félix Candela and Heinz Isler: a comparison of two structural artists. In: Adriaenssens S, Block P, Veenendaal D, Williams C (eds) Shell structures for architecture: form finding and optimization. Routledge/ Taylor & Francis Group
33. Dubor A, Cabay E, Chronis A (2018) "Energy Efficient Design for 3D Printed Earth Architecture," in *Humanizing Digital Reality: Design Modelling Symposium Paris 2017*, De Rycke K, Gengnagel C, Baverel O, Burry J, Mueller C, Nguyen MM, Rahm P, Thomsen MR Eds., Singapore: Springer, pp. 383–393. https://doi.org/10.1007/978-981-10-6611-5_33
34. Curth A, Darweesh B, Arja L, Rael R (2020) Advances in 3D printed earth architecture: on-site prototyping with local materials. BE-AM Symposium 2020. BE-AM | Built Environment - Additive Manufacturing, Darmstadt Germany
35. Gericke O, Kovaleva D, Haase W, Sobek W (2016) "Fabrication of Concrete Parts using a Frozen Sand Formwork," in *Spatial Structures in the 21st Centruy*, Tokyo. [Online]. Available: https://www.researchgate.net/publication/309464716_Fabrication_of_Concrete_Parts_using_a_Frozen_Sand_Formwork
36. Sitnikov V (2019) Ice formwork for high-performance concrete: a model of lean production for prefabricated concrete industry. Structures 18:109–116. https://doi.org/10.1016/j.istruc.2018.11.004

37. Li W, Lin X, Bao DW, Min Xie Y (2022) A review of formwork systems for modern concrete construction. Structures 38:52–63. https://doi.org/10.1016/j.istruc.2022.01.089
38. Hurkxkens I, Mirjan A, Gramazio F, Kohler M, Girot C (2020) "Robotic Landscapes: Designing Formation Processes for Large Scale Autonomous Earth Moving," in *Impact: Design With All Senses: Proceedings of the Design Modelling Symposium, Berlin 2019*, Gengnagel C, Baverel O, Burry J, Ramsgaard Thomsen M, Weinzierl S Eds., Cham: Springer International Publishing. https://doi.org/10.1007/978-3-030-29829-6
39. Bureau of Indian Standards (2000) IS 456: Plain and Reinforced Concrete - Code of Practice
40. International Code Council. (2020). 2021 International building code (IBC): chapter 18 soils and foundations. International Code Council, Inc.
41. Kurian NP (2004) Design of foundation systems: principles and practices, 3rd edn. Alpha Science International Ltd.
42. Feickert K, Mueller CT (2023) Algorithmic investigation of structural system utility for urban development reusing existing foundations. IASS Annual Symposium 2023. Integration of Design and Fabrication, Melbourne, Australia
43. D'Amico B, Pomponi F (2020) On mass quantities of gravity frames in building structures. J Build Eng 31:101426. https://doi.org/10.1016/j.jobe.2020.101426
44. C-Change Labs (2011) "Embodied Carbon in Construction Calculator (EC3) Tool." Building Transparency.Accessed: Aug. 11, 2021. [Online]. Available: https://buildingtransparency.org/ec3
45. De Wolf C, Ramage M, Ochsendorf J (2016) Low carbon vaulted masonry structures. J Int Assoc Shell Spat Struct 57(4):275–284. https://doi.org/10.20898/j.iass.2016.190.854
46. Foraboschi P, Mercanzin M, Trabucco D (2014) Sustainable structural design of tall buildings based on embodied energy. Energy Build 68:254–269. https://doi.org/10.1016/j.enbuild.2013.09.003
47. Oval R, Nuh M, Costa E, Madyan OA, Orr J, Shepherd P (2023) A prototype low-carbon segmented concrete shell building floor system. Structures 49:124–138. https://doi.org/10.1016/j.istruc.2023.01.063
48. Moussavi Nadoushani Z, S., Akbarnezhad A. (2015) Effects of structural system on the life cycle carbon footprint of buildings. Energy Build 102:337–346. https://doi.org/10.1016/j.enbuild.2015.05.044